On the account of a cohesive interface for modeling the behavior until break of highly filled elastomers

Paul-Aymé Toulemonde[a,b,*], Julie Diani[a], Pierre Gilormini[a], Nancy Desgardin[b]

[a]*Laboratoire PIMM, CNRS, Arts et Métiers ParisTech, 151 bd de l'Hôpital, 75013 Paris, France*
[b]*Herakles groupe Safran, Centre de recherche du Bouchet, 9 rue Lavoisier, 91710 Vert-le-Petit, France*

Abstract

The nonlinear behavior and failure of highly filled elastomers are significantly impacted by the volume fraction, the size and nature of fillers and the matrix stiffness. Original experimental data obtained on glass beads reinforced acrylates and on propellants allow illustrating and discussing the main effects generally observed. In order to better understand the effects of the microstructure and constitutive parameters on the behavior and failure of highly filled elastomers, a composite model, represented by a 2D periodic cell with randomly dispersed particles, with an account of a cohesive zone at the filler/matrix interface is used. Finite element simulations with finite strain provide insight on the stress-strain responses dependence to the model parameters and allow defining a failure criterion perceived by the appearance of a critical fibrillar microstructure.

[*]Corresponding author. Tel. : + 33 1 44 24 65 74
Email address: `paul-ayme.toulemonde@ensam.eu` (Paul-Aymé Toulemonde)

1. Introduction

Solid propellants are made of polymer networks in the rubbery state filled with a very large amount of rigid oxidizer and metal fillers (volume fraction ranging between 50% and 90%). In an attempt to develop new materials, it is often desired to improve both strain and stress at failure. In order to comply with such a challenge it is necessary to understand the impact of the various material parameters on the propellant mechanical behavior. When narrowing our interest to the damage and failure, neglecting the viscoelasticity, of highly filled elastomers (discarding thermoplastic matrices) containing micrometric particles (eliminating nanosize particles like carbonblack or silica fillers), experimental data are scarce in the literature. One may cite the work of Vratsanos and Farris (1993a), reporting experimental data featuring the effect of the amount of fillers, the size of the fillers and the strength of the adhesion at the filler/matrix interface on the behavior and failure of glass bead reinforced polyurethane composites. Since damage at the filler/matrix interfaces, recognized as matrix debonding also named dewetting, seems to affect significantly the behavior of such composites, account for cohesive zones at the filler/matrix interfaces is often used to model the behavior of such materials following either a micromechanics approach or a finite element numerical approach. Micromechanics modeling is found in the case of linear material response and infinitesimal strain (Dvorak and Zhang, 2001; Tan et al., 2005; Nie and Basaran, 2005; Inglis et al., 2007; Tan

2

et al., 2007, Ngo et al., 2010), and nonlinear hyperelastic matrix behavior for moderate amount of fillers (Brassart et al., 2009). The main limits of the micromechanics approach rest on the complications raised by the nonlinear behavior of the elastomer matrix, the large deformation that it may be submitted to, the very high volume fractions of fillers, and on the difficulty to define a local criterion for matrix failure that is sensitive to the field heterogeneities induced by the microstructure. Various finite element formulations have been proposed (Zhong and Knauss, 1997; Zhong and Knauss, 2000; Matouš and Geubelle, 2006, Matouš et al., 2007; Moraleda et al., 2009, Ngo et al., 2010). Early papers (Zhong and Knauss, 1997; Zhong and Knauss, 2000; Matouš and Geubelle, 2006, Matouš et al., 2007) focus on the numerical feasibility and the effect of cohesive zones on the composite stress-strain behavior. Zhong and Knauss (1997, 2000) show interest in the impact of the size of particles and of the interactions between particles for simple cells containing four particles arranged in a square manner. Moraleda et al. (2009) have proposed an interesting study on the impact of the strength and toughness of the cohesive zones but that lacks a discussion of the length scale parameters, which is essential when accounting for cohesive zones. Finally, Ngo et al. (2010) were also interested in the effects of the model and microstructure parameters but limited their study to the case of a single filler within a matrix of linear behavior undergoing infinitesimal strain.

In the current contribution, it is proposed to look at the general characteristics of the uniaxial behavior until break of highly filled elastomers at the light of existing and original experimental data, and to draw a qualitative comparison between the highlighted tendencies and those obtained by finite

3

element simulations on periodic cells containing randomly distributed rigid particles in a hyperelastic matrix with a cohesive zone at each filler/matrix interface. A two dimensional numerical study of the microstructure and constitutive parameters is carried out to better recognize the key parameters that could enhance the strain and stress at break of such composites. Finally, criteria for composite failure are enunciated for simulations.

2. Experimental evidences on the monotonic behavior of highly filled elastomers

This section aims at reporting the effects of the material parameters on the uniaxial tensile stress-strain response of highly filled elastomers. Since experimental data are scarce, it was decided to present original experimental data that would help discussing the results of the literature.

2.1. Materials

2.1.1. Solid propellants

Solid propellants such as produced by Herakles groupe Safran were considered. In order to test the effect of the particle size, a plasticized elastomer was reinforced by explosive organic fillers called A with two different granulometries, either centered around 3 μm of diameter with very small scatter or centered around 26 μm of diameter with a wide scatter. Materials with 49% and 61% volume fractions of filler were prepared. In order to test the impact of the adhesion at the filler/matrix interface, another plasticized elastomer was mixed with either filler A or filler B, the latter being expected to enhance the polymer adhesion at its surface. The distribution of diameters for the

4

filler B was similar to the second granulometry of filler A: centered around 26 μm with equally wide scatter. Finally, two matrices with significantly different behaviors were reinforced by the same amount and same type of filler (A) to study the effect of the matrix stiffness on the behavior of the composite. Tests were conducted at room temperature on 1 cm wide, 4 cm long and 0.5 cm thick dog-bone samples on a Zwick Z1.0 machine with a 1 kN load cell. For each material, five samples were tested.

2.1.2. Polyacrylate/glass beads composites

In order to avoid limiting ourselves to propellants, acrylate networks reinforced by micrometric glass beads were also prepared. Based on the tailorability of these networks (Safranski and Gall, 2008), the polymer network consists in a mix of 98 mol% Benzyl-methacrylate (BMA) monomer with 2 mol% Poly(ethylene glycol) dimethacrylate (PEGDMA) (550 g/mol) crosslinker copolymerized by UV reaction thanks to the 2,2-Dimethoxy-2phenylaceto-peone photoinitiator. All products were used as received by Sigma-Aldrich. Sodocalcic glass beads with diameters in the range 45-63 μm were added as fillers. Final products are plates of 1.5 mm thickness after 55 min of curing within a UV chamber CL-1000. Dog-bone samples of 50 mm length and 4 mm width were punched from the plates and tested in uniaxial tension at 20°C above the glass transition temperature in the rubbery state, on an Instron 5881 tensile machine equipped with an Instron thermal chamber and a 1kN load cell.

For the acrylate composites as for the propellants, due to the large strain involved, the strain is measured locally with video extensometers during the tensile tests. Experimental tests were run at least three times for each ma-

terial in order to assess the reproducibility of the experimental results that are presented below.

2.2. Effect of the filler volume fraction

The experimental data from Figure 1 in Vratsanos and Farris (1993b) are often used as reference data describing the effect of the amount of fillers on the mechanical behavior of elastomers reinforced by spherical particles. Polyurethane composites containing from 0% to 50% of glass beads were tested by these authors in uniaxial tension while measuring the sample volume change. As expected, the initial modulus depends on the filler volume fraction. The onset of damage, detected by an increase of the sample volume, appears at a smaller macroscopic strain when the amount of filler increases. Finally, the strain at break decreases with the increase of the amount of filler. The impact of the amount of filler was also tested on our acrylate/glass bead composites. One notes in figure 1 that the same general characteristics as reported by Vratsanos and Farris (1993b) are obtained. Nonetheless, we can point out one major difference. The specific wavy shape of the stress-strain response displayed by the material reinforced by 40% of particles in Vratsanos and Farris (1993b) is not obtained here. Actually, a similar shape has been obtained once but without being representative of the behavior of the material at the tested volume fraction. Moreover, it was noted that experimental data from Figure 1 of Vratsanos and Farris (1993b) are mentioned to have been initially reported by Yilmazer and Farris (1983), who dealt with aged composite matrix and did not present the data plotted by Vratsanos and Farris (1993b).
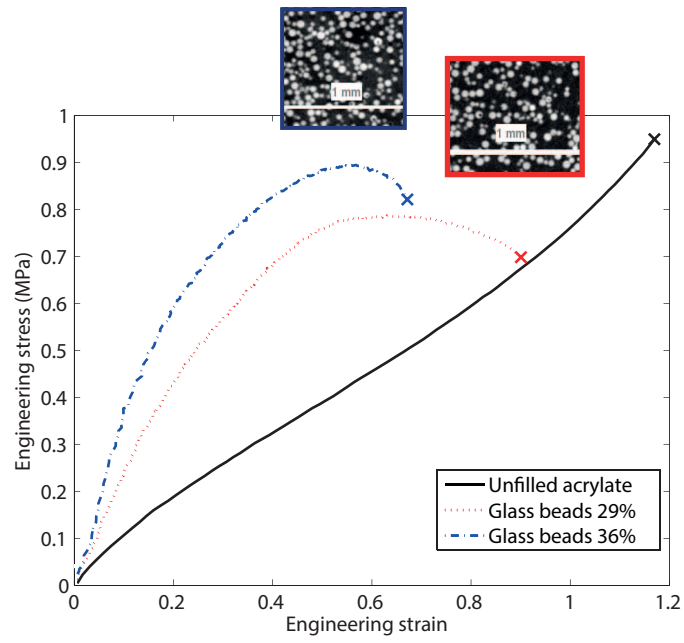
Figure 1: Uniaxial tension stress-strain behavior of polyacrylate/glass beads composites with respect to the volume fraction of filler. Tomography images of the corresponding materials (insets) also illustrate the particle volume fraction.
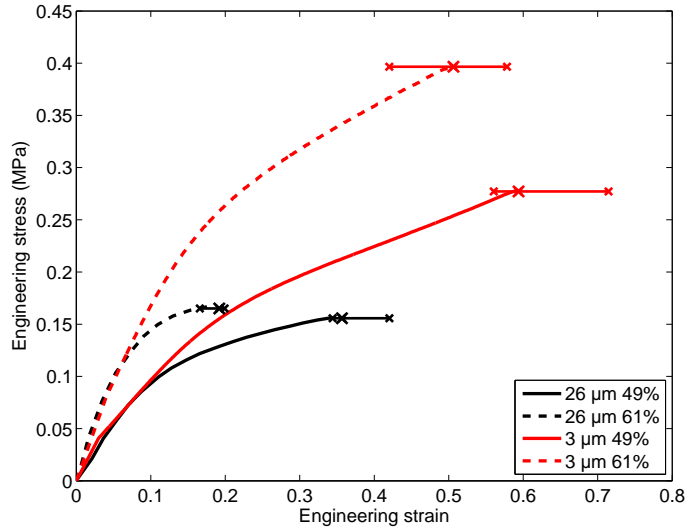
Figure 2: Uniaxial tension stress-strain behavior of filler A reinforced propellants for various particles sizes.

2.3. Effect of the particles size

Vratsanos and Farris (1993a) have tested the effect of the particles size in their polyurethane composites reinforced by glass beads. They show that the initial modulus of the composites does not depend on the particles size, and that both the stress for damage onset and the strain at break increase significantly for smaller particles. We obtained similar experimental properties on propellants. Figure 2 shows the uniaxial stress-strain responses of propellants made of the same rubber matrix containing the same type of fillers but with different granulometries for 49% and 61% of volume fractions. From figure 2 the same conclusions as exposed by Vratsanos and Farris (1993a) can be drawn.
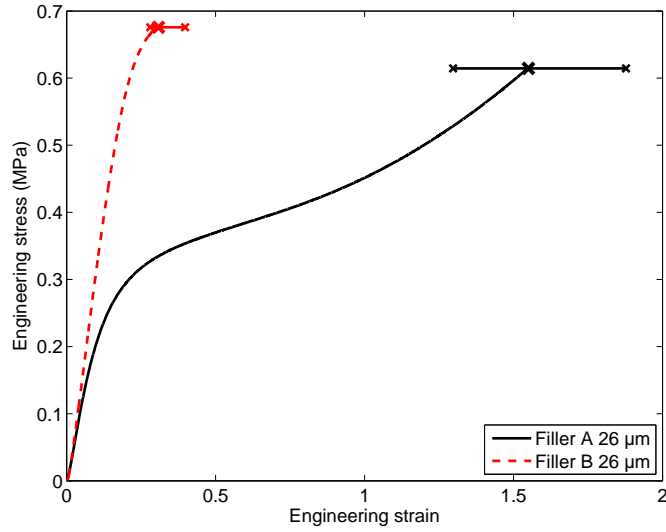
Figure 3: Uniaxial tension stress-strain behavior of filler A or B filled propellants illustrating the impact of the nature of the adhesion at the filler/matrix interface.

2.4. Effect of the adhesion at the filler/matrix interface

Vratsanos and Farris (1993a) reported that when the adhesion between the matrix and the particles is good, damage appears later and remains small before catastrophic failure occurs, the strain at failure being considerably reduced. In order to test the adhesion at the filler/matrix interface, two materials differing by the type of fillers only have been tested in uniaxial tension (figure 3). The filler volume fraction is 60% in both materials, which explains similar initial moduli. The composite with filler B presents the characteristics of a better adhesion at the filler/matrix interface and displays an early failure just following the onset of damage.
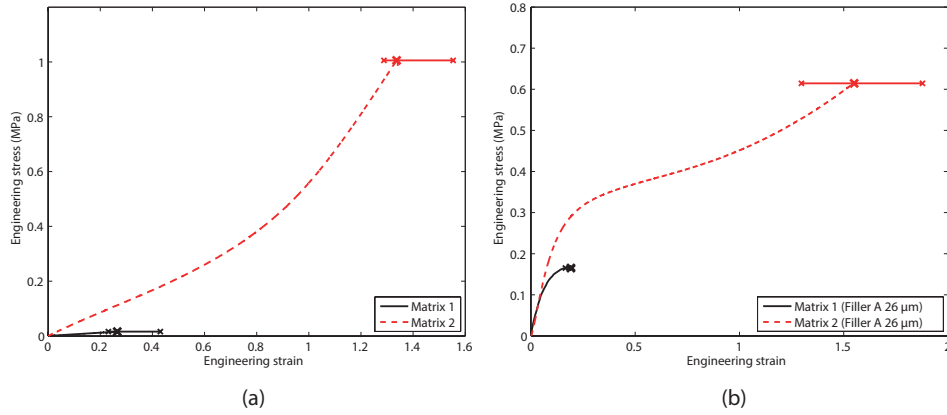
Figure 4: Uniaxial tension behaviors of two propellants matrices (a) and of the two corresponding propellants filled with filler A (b).

2.5. Effect of the matrix behavior

Two propellant matrices differing by their initial modulus and uniaxial toughness (figure 4) were reinforced with the same filler A whose size distribution is centered around 26 μm. Both propellants were tested in uniaxial tension. Figure 4 shows the effects of a stiffer matrix on the composite behavior, including a larger initial modulus and a larger stress at damage onset. The larger strain and stress at failure obtained for the composite with the stiffest matrix may be due to the larger toughness of this matrix, even though it was observed that the limit properties of a propellant are not necessarily improved by increasing its matrix toughness.

2.6. Evidence of filler/matrix dewetting

Since Oberth and Bruenner (1965), experimental evidence of dewetting between matrix and filler in a elastomer filled with microsize particles has been provided. Tao et al. (2013) report the same mechanism in propellants

and emphasized the appearance of these voids primarily around larger particles. The matrix being hyperelastic, it retracts upon failure and therefore voids cannot be observed through *post-mortem* studies. In-situ experiments or quenchable materials are required. Figure 5 presents images obtained with a Hitachi S-4800 SEM of quenched samples of the polyacrylate/glass beads composite with filler volume fraction of 36% detailed above at different macroscopic strains: 10%, 20% and 50%. At 10% (figure 5a) voids around filler particles cannot be clearly identified. At 20% (figure 5b) small voids have appeared in the loading direction and they expand greatly at 50% strain (figure 5c). At 50% strain, one can also notice the appearance of highly stretched matrix fibrils in the loading direction and between voids. These observations underline the need to account for particle/matrix dewetting in order to capture the damaging process in these composites.

3. Model

A two-dimensional model is studied in order to gain insight on the key parameters that have an impact on the failure of the composite. The results are compared qualitatively to the tendencies highlighted by experimental data.

3.1. Matrix behavior and cohesive zone model

The matrices of propellants are made of amorphous polymer networks used well above their glass transition in the rubbery state. They can be significantly stretched and can be modeled by an incompressible hyperelastic strain energy density. Considering the simple neo-Hookean law, $\mathcal{W} = C_0(I_1 - 3)$ (I_1 being the first invariant of the right Cauchy-Green tensor), the matrix
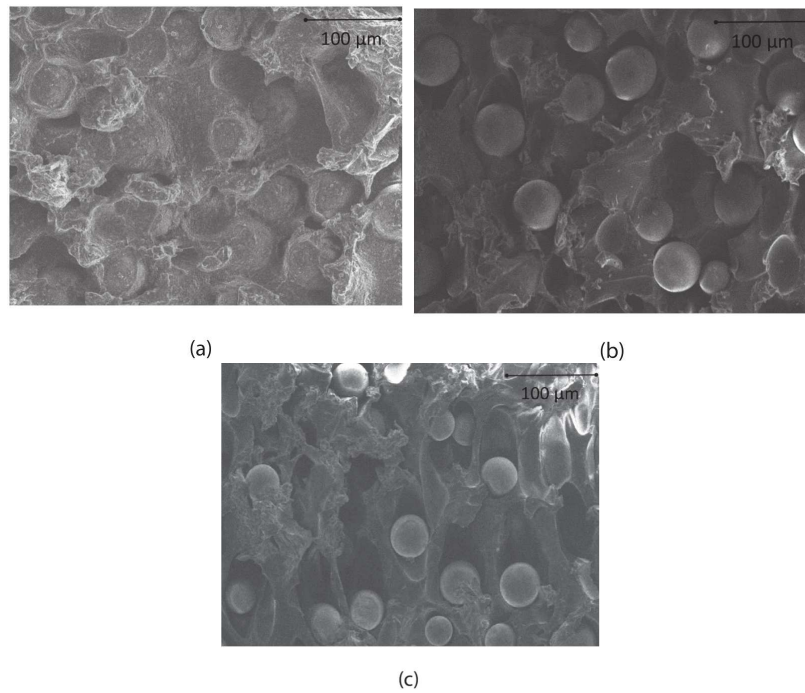
Figure 5: Hitachi S-4800 SEM micrographs of 36% glass beads filled polyacrylate quenched at different strain: (a) 10%, (b) 20% and (c) 50%. The loading direction is vertical for each image.
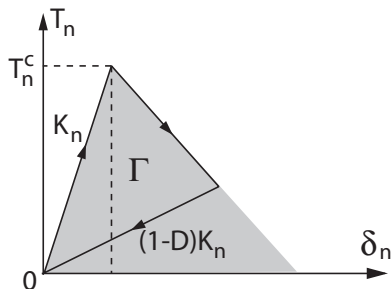
Figure 6: Illustration of the cohesive zone model for a purely normal displacement.

is characterized by the parameter $C_0 = E/6$ with E its Young modulus at small strain. Note that other hyperelastic strain energy densities may be chosen without changing the qualitative aspects of the results that are presented in this contribution, as shown in section 4.6. As to the fillers, they can be assumed rigid when comparing their stiffness to the matrix stiffness.

A cohesive zone model (CZM) is used to describe the evolutive adhesion at a filler-matrix interface (see the critical review by Park and Paulino, 2011). Figure 6 displays the bilinear traction-separation model used here in the case of a purely normal diplacement δ_n, with the initial stiffness denoted K_n. Once a critical stress T_n^c is reached, the matrix-filler debonding degrades the interface stiffness, which decreases progressively until becoming null when the supplied work per unit interface area reaches the critical value Γ (gray area in Figure 6). More generally, the CZM model used here is available in Abaqus (2011) code; it is adapted from Camanho et al. (2003) but is not fully documented. A series of tests applying various loading paths allowed to detail this model as follows. With δ_n and δ_t denoting the normal and tangent components of the relative displacement of the material with respect to the substrate in the contact zone, the nondimensional variable

13

$\alpha = \sqrt{(K_n\,\delta_n/T_n^c)^2 + (K_t\,\delta_t/T_t^c)^2}$ is defined, where K_n and K_t are the stiffnesses of the undamaged cohesive zone in the normal and tangent directions, T_n^c and T_t^c are given critical stresses for damage onset in purely normal and purely tangent displacements, respectively. Moreover, $\alpha_m = \max\{\alpha_m, \alpha\}$ denotes the largest α value reached and $\alpha_f = \min\{1, (K_n\,\delta_n^2 + K_t\,\delta_t^2)/(2\alpha\Gamma)\}$ is updated when α_m is updated (i.e., when $\alpha = \alpha_m$). The interface damage D keeps its initial zero value as long as $\alpha_m \leq 1$, otherwise

$$D = \frac{\alpha_m - 1}{\alpha_m - \alpha_f} \tag{1}$$

with $D = 1$ (fractured interface) obtained when $\alpha_f = 1$, and the components of the traction vector at the interface are

$$T_n = (1 - D)K_n\,\delta_n \qquad \text{and} \qquad T_t = (1 - D)K_t\,\delta_t\,. \tag{2}$$

The above equations assume that $T_n \geq 0$, but variants can be defined like in Camanho et al. (2003) to account for a compressive traction at the interface. This formulation of the cohesive zone model involves 5 independent material constants (K_n, K_t, T_n^c, T_t^c and Γ) and ensures that the adhesive energy is equal to Γ for any loading that keeps a constant ratio between δ_n and δ_t. Moreover, the formulation of Camanho et al. (2003) for the special case $G_{Ic} = G_{IIc}$ is recovered if $K_n = K_t$. For nonproportional loadings (a normal displacement followed by a tangent displacement, for instance), the dissipated energy when the interface is fractured may differ from Γ, unless the additional constraint $T_n^c/T_t^c = \sqrt{K_n/K_t}$ is satisfied by the material constants. In these conditions, T_n and T_t can be shown to derive from a potential, and the formulation of Tvergaard and Hutchinson (1993) applied to a bilinear law is recovered.

3.2. Representation of the composite microstructure

Model materials were designed for finite element simulations, where fillers were schematized by parallel circular cylinders with identical radii R. This allowed meshing merely a section of the material. The created microstructure is periodic, and the unit cell contains a random distribution of 49 disks. The algorithm given by Torquato (2002) has been used to obtain such distributions, and an example is shown in figure 7, where the boundary of each black area defines a cohesive zone. The randomness of the microstructure can be estimated by computing the autocorrelation function $S_2(h)$ where h is the length of the probe vector (Torquato, 2002), and figure 7 presents a comparison of its average over four directions (0, 45, 90 and 135 degrees) for the displayed cell, which compares satisfactorily with the exact solution for an infinite and perfectly disordered composite calculated by Torquato and Lado (1985). Periodic boundary conditions are applied to the unit cell to prescribe uniaxial tension along either the vertical or the horizontal axis, in plane strain. Finally, each simulation is performed on 4 different random microstructures each in two directions which make 8 different calculations, in order to account for the scatter introduced by randomization. Note that except when stated otherwise, the considered microstructures contained 50% volume fraction of fillers.

The simulations were run in finite strain with Abaqus/Standard. The meshes used 4-node hybrid plane strain elements with reduced integration. Around 270,000 elements were used to mesh the matrix in each microstructure. In order to obtain a smooth propagation of damage at the filler/matrix interfaces, the distance between two nodes along the cohesive zone was cho-
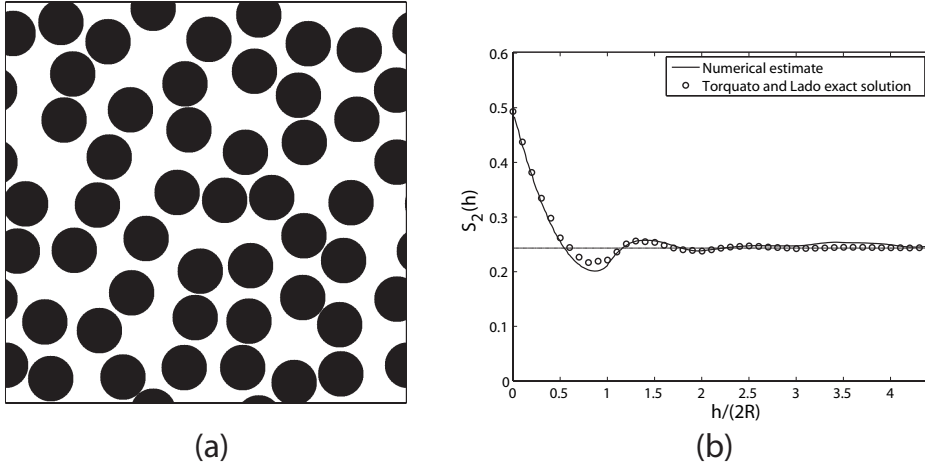
15

Figure 7: Example of a 2D random cell (a) and its autocorrelation function with h the probe vector length and R the particle radius (b).

sen at least 7 times (and more often 10 times) smaller than the displacement for interface failure. The C_0 parameter of the neo-Hookean matrix behavior was taken equal to 2.2 MPa, and the parameters used to define the cohesive zone model were $K_n = 3K_t = 1500$ MPa, $T_n^c = T_t^c = 3.3$ MPa and $\Gamma = 0.25$ MPa.mm. Therefore, interface failure is obtained for the same purely normal or purely tangent displacement of 0.15 mm, which provides a material length δ^f to be compared to the particles diameter. These are the reference values for all calculations below, on which the effects of variations are studied. These values for matrix and cohesive zone parameters are in the same range as those used by Tan et al. (2007).

16

4. Composite behavior and failure

4.1. Failure criteria

When a unit cell with randomly dispersed fillers is submitted to uniaxial tension, a typical two-step microstructural evolution is observed. First, matrix debonding occurs quite homogeneously over the particles, with damage remaining moderate, then an instability localizes along a strip of particles aligned orthogonally to the tensile direction, and damage increases dramatically. An illustration of this characteristic two-step microstructure evolution is shown in figure 8. Once instability occurs, the elastomer matrix in the strip is strained severely and fibrils are formed, while the composite parts on each side of the fibrils zone tend to move as rigid bodies. Such strain localization has been observed experimentally by Liu et al. (2004). The appearance of the fibrillar microstructure may define a criterion for the occurrence of a catastrophic crack causing the failure of the composite. Nonetheless, we encountered situations for which it could be difficult to detect the fibrillar microstructure and a strain energy criterion for matrix failure was defined alternatively. Such a criterion is inspired from the fracture mechanics theory and has been used extensively (Rivlin and Thomas 1953). A critical strain energy of 10.9 MPa could be chosen by recording the maximum strain energy when fibrils appeared during the simulation of a tensile test performed on a random microstructure. Therefore, two criteria are used below for material failure: an instability criterion recognized by the localization of strain in a fibrillar microstructure, and an energy criterion reached when the maximum strain energy within the matrix reaches the value 10.9 MPa. In the next section, both criteria are applied to random cells submitted to uniaxial tension

17

and the results are compared to the experimental trends reported in section 2 in order to discuss their relevance.

4.2. Damageable behavior

Figure 9 illustrates the uniaxial stress-strain responses of eight cells with different layouts of particles for the reference set of parameters. Both failure criteria are applied. First, it appears that the stress-strain curve and the fracture behavior achieve very good reproducibility except for one structure. This means that applying the chosen process to create eight microstrutures is enough to reach representative mechanical responses and fracture for this set of material parameters in uniaxial tension. Hence, a median behavior will be represented for each set of tested parameters. Second, upon loading, the applied displacement is accommodated by strain within the matrix and/or by matrix debonding at the matrix/filler interface. As the dilatation of the cells in figure 9 suggests, no dilatation occurs in the first phase of the stress-strain response (from 0 to 0.05 strain), which means that no matrix debonding occurs. Thus, in this phase, the matrix supports the load while the cohesive zone at the matrix/filler interface remains in its elastic part. The quadratic stress criterion for the cohesive zone has not yet been reached. In the second phase (over 0.05 strain) both dilatation and softening of the composite occur simultaneously. This is due to gradual filler/matrix debonding.

Figure 10 represents an histogram of the particle fraction as a function of the nearest neighbor distance (NND) for the reference set of simulation parameters. An average over the eight structures simulated in figure 9 is represented for two cases where either all particles in the cell are reported or only the particles involved in the band of localized debonding are reported.
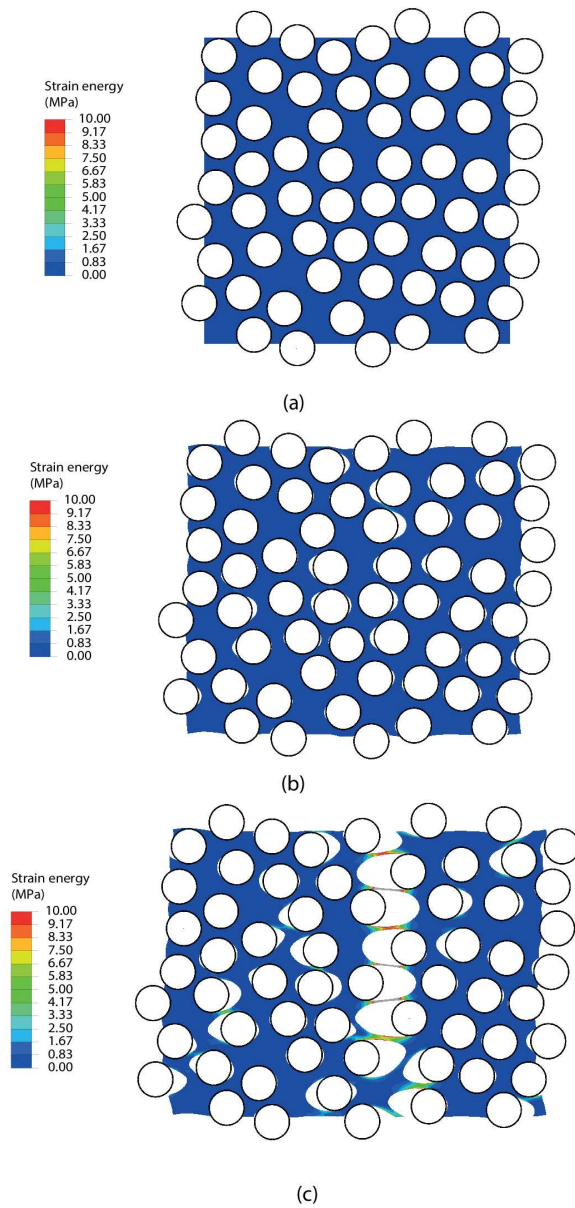
18

Figure 8: Evolution of a cell with reference microstructural and material parameters submitted to uniaxial tension. (a) Initial microstructure, (b) early evolution with matrix debonding homogeneously distributed over the particles, and (c) further damage evolution with the appearance of matrix fibrils.
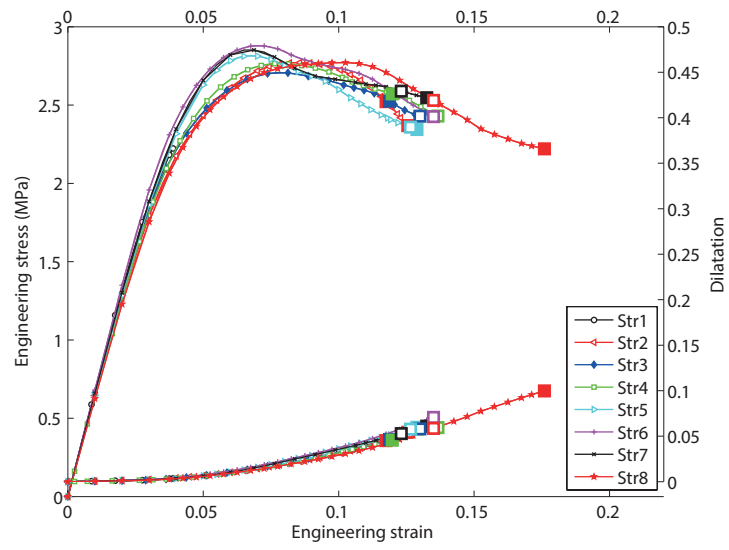
Figure 9: Composite behavior and failure in uniaxial tension for various microstructures. Open squares correspond to the energy criterion being satisfied and filled squares indicate the appearance of a fibrillar microstructure. Upper curves represent the mechanical behavior and lower curves represent the relative volume change.
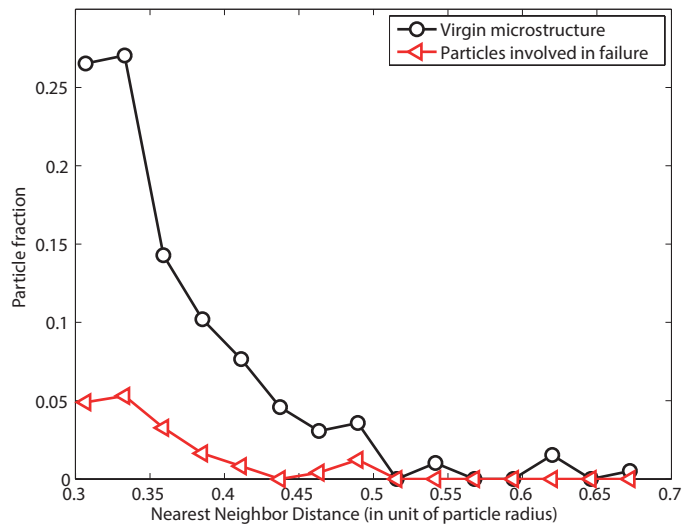
Figure 10: Histogram showing average particle fractions measured on 8 microstructures as a function of the nearest neighbor distance expressed in unit of particles radius in the cases where either all particles are reported or only particles involved in the band of localized debonding are reported.

This kind of representation is inspired from Ghosh et al. (2000) and leads to a similar conclusion: the failure path foremostly encompasses particles with the smallest NND. However, due to screening effects between particles, the failure path does not encompass particles with the smallest NND only but particles with a larger NND are also involved. Moreover, due to the high filler volume fraction, over 95% of the particles have a NND in the range 0.3-0.5 in unit of particle radius, which is not as discriminative as in Ghosh et al. (2000).

4.3. Effect of the filler volume fraction

The failure criteria are then tested on microstructures filled with various volume fractions of particles. Each random microstructure contains 49 fillers of the same radius and the constitutive parameters of the cohesive zone and of the matrix are identical, only the size of the cell changes. Figure 11 shows the effect of the volume fraction on the composite behavior and failure. As expected, the initial modulus increases with the increase of the amount of fillers. First, one notices also that voids appear earlier and increase faster for the material containing the larger amount of fillers. The latter result is consistent with the observation reported by Vratsanos and Farris (1993a). Second, both energy and microstructure failure criteria appear as equivalent. Since failure is due to the appearance of fibrillar microstructures in all these calculations and the numerical value for the energy failure criterion was chosen from one of them, the correspondence between both criteria was expected. Third, the simulations show the strain at failure that decreases when the amount of filler increases, which is consistent with experimental data, albeit it is more obvious on the experimental data (Figure 1).
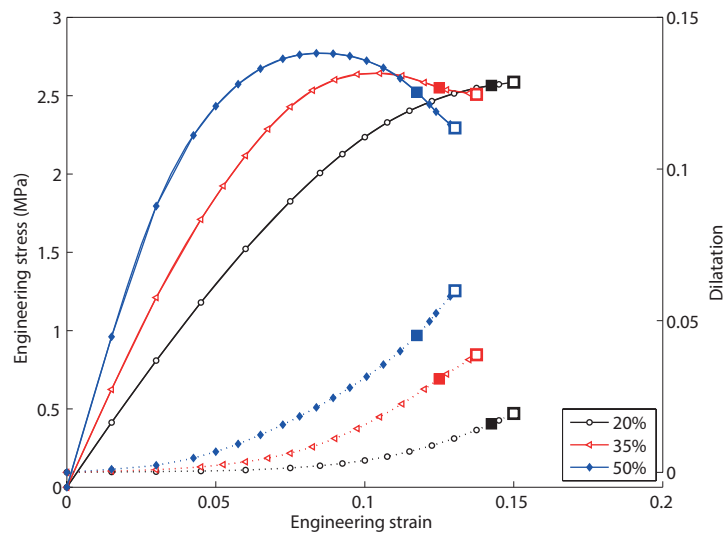
22

Figure 11: Behavior and failure of the model filled elastomers with respect to the volume fraction of fillers. Open squares correspond to the energy criterion being satisfied and filled squares indicate the appearance of a fibrillar microstructure. Upper curves represent the mechanical behavior and lower curves represent the relative volume change.

4.4. Impact of the length parameters on the composite failure

The impacts of the cohesive zone length parameters δ^f ($\delta^f = 2.\Gamma/T^c$) and R on material failure are tested. First, figure 12 shows the responses and the volume changes of random composites submitted to tensile tests for different values of δ^f. In this case it appears that both failure criteria are equivalent. Since the interface strength T^c is identical in all calculations and δ^f varies, the decohesion energy increases when δ^f increases. Damage at the interface starts at the same overall strain in all cases since T^c does not vary. For the largest value of δ^f, which simulates the slowest damage at the filler/matrix interface, the composite failure occurs at the largest strain and stress. When δ^f is smaller, full damage at the filler/matrix interface is rapidly completed and the fibrillar microstructure appears. Therefore, increasing significantly the toughness at the filler/matrix interface delays the catastrophic failure of the composite.

Next, the matrix/filler adhesion properties were assumed constant while the size of the fillers was changed. Figure 13 presents the behavior and failure of random microstructures according to the size of the fillers, the volume fraction of fillers remaining equal to 50%. First, one notices that for small particles the initial modulus is smaller, this is due to the stress contribution of the cohesive zone which depends on the local displacement rather than the local strain. In order to represent a composite material with smaller particles but still containing 50% of fillers, both the cell and particle sizes are smaller and, consequently, local displacements are smaller at a given strain of the cell. For large fillers, the appearance of a fibrillar microstructure was never clearly detected since dewetting at the matrix/filler interface was
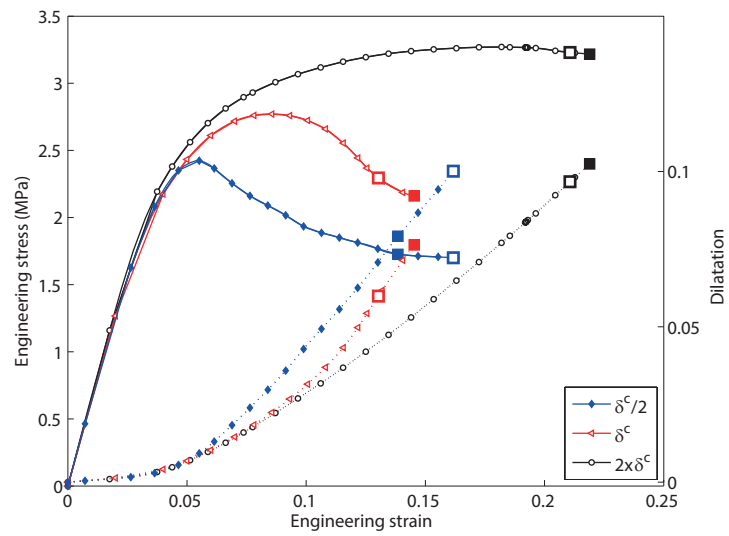
24

Figure 12: Composite behavior and failure in uniaxial tension for various values of the CZM critical displacement. Open squares correspond to the energy criterion being satisfied and filled squares indicate the appearance of a fibrillar microstructure. Upper curves represent the mechanical behavior and lower curves represent the relative volume change.
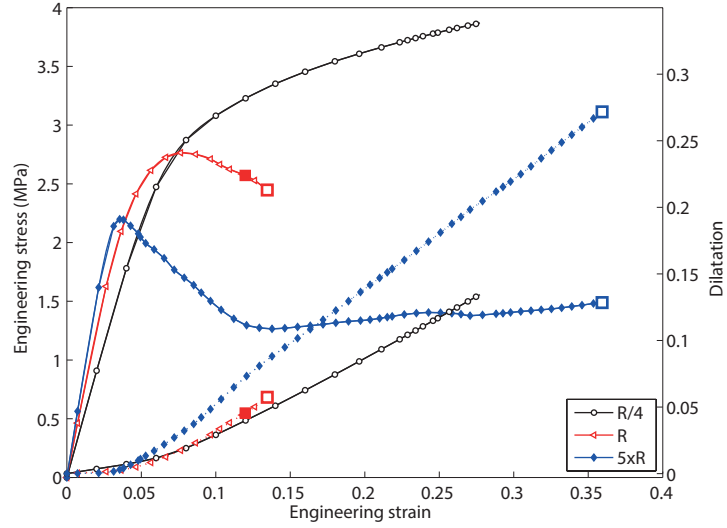
Figure 13: Composite behavior and failure in uniaxial tension for various sizes of fillers. Open squares correspond to the energy criterion being satisfied and filled squares indicate the appearance of a fibrillar microstructure. Upper curves represent the mechanical behavior and lower curves represent the relative volume change.

homogeneously distributed over the microstructure. The energy criterion is obtained at a very large strain, which raises the question of the relevance of the energy criterion when no fibrillar microstructure exists.

4.5. Impact of the critical stress of the CZM

The effect of the filler/matrix interface strength is tested by varying the damage initiation stress T^c (which modifies δ^f the opposite way, since Γ is kept constant). Figure 14 shows the mechanical behaviors and volume changes recorded with random microstructures for various T^c values. Increasing the interface strength reduces the cavity formation at the filler/matrix interfaces, thus enhancing the reinforcement effect of the fillers and the stresses in the matrix; the energy criterion for failure is satisfied rapidly. To the con-

trary, decreasing T^c favors matrix dewetting at the filler/matrix interfaces, which reduces the particle reinforcement effect and the strain in the matrix, since void growth accommodates a part of the applied strain. As a consequence, the interface strength has opposite effects on the stress and strain at failure.

In an attempt to compare these results with experimental data in figure 3 dealing with different filler/matrix interactions, one notes that in figure 3 strain at failure is largely reduced for composite B. According to figure 14, this would be consistent with an increase of the critical strength at the filler/matrix interface. None of the simulations were able to reproduce the behavior and stress at failure of composite A, which may result from changes of both interface strength and toughness.

4.6. Impact of the constitutive law of the matrix

The effect of matrix properties on the response of the composite is tested by varying the form of its stress-strain response and its initial stiffness.

Figure 15 presents the effect of an upturn in the matrix model (figure 15a) on the composite response (figure 15b). To obtain this upturn, an Arruda-Boyce hyperelastic model is used. The initial stiffness is constant in every case but the asymptotic strain of the upturn is varied. This translates into a same stress-strain response of the composite at low strain but various failure strains. As figure 15b demonstrates, the upturn has little influence on the failure behavior of the composite if the asymptotic strain is high enough. This suggests that only the matrix stiffness values up to 0.5 strain is significant in the present condition, not the shape of the matrix model.

Finally, the effect of the matrix stiffness on the composite failure can be
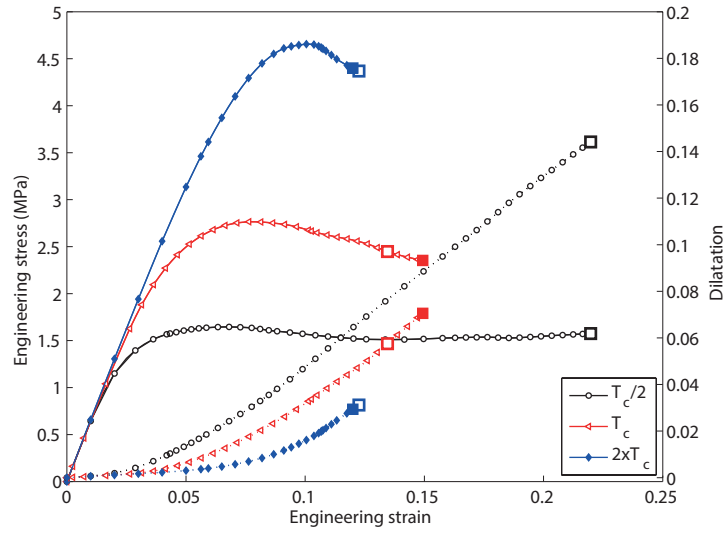
Figure 14: Composite behavior and volume change in uniaxial tension for various CZM strengths at the filler/matrix interface. Open squares correspond to the energy criterion being satisfied and filled squares indicate the appearance of a fibrillar microstructure. Upper curves represent the mechanical behavior and lower curves represent the relative volume change.
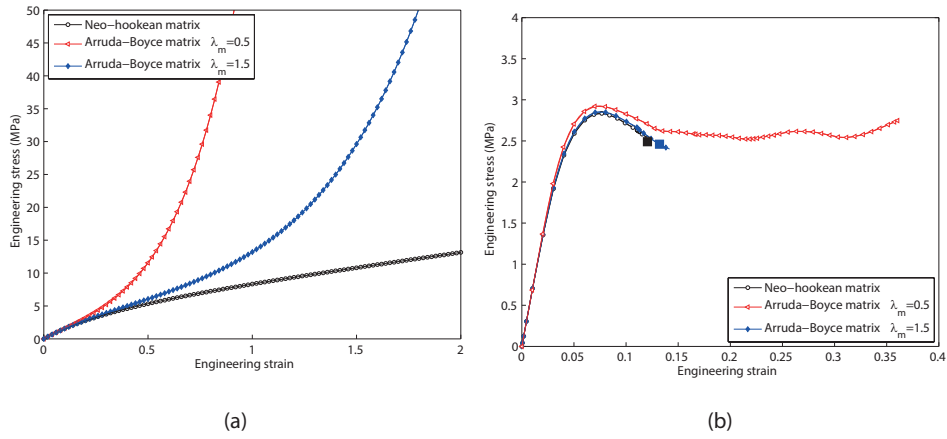

Figure 15: (a) Matrix models considered (uniaxial tension) and (b) effect of an upturn in the matrix model on the stress-strain response and failure of the composite in uniaxial tension. Only the failure criterion based on the appearance of matrix fibrils is plotted.
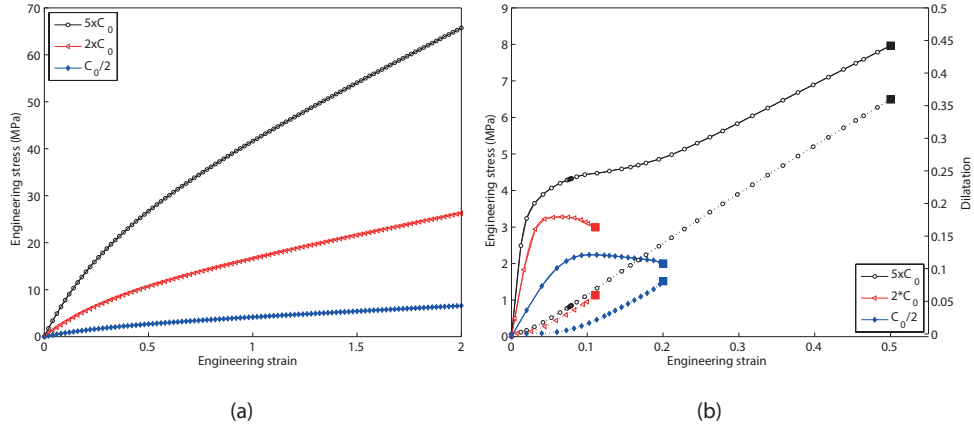
28

Figure 16: Effects of the matrix stiffness on the stress-strain response and failure of the composite: (a) matrix behavior, (b) composite response (upper curves represent the mechanical behavior and lower curves represent the relative volume change). Only the failure criterion based on the appearance of matrix fibrils is considered.

evaluated by applying the fibrillar microstructure criterion only, since there is no unequivocal relation between stiffness and critical elastic energy density for elastomers. Figure 16a illustrates the stress-strain response for the chosen values of the parameter C_0 and figure 16b shows the corresponding behavior and volume change of a random composite. One notes that both the composite stress and strain at failure are significantly improved when C_0 is increased substantially, which is due to the filler/matrix debonding spreading over the whole microstructure and limiting strain localization. These numerical results are consistent with the experimental observations reported in figure 4.

29

5. Conclusion

Highly filled elastomers, like propellants, have been modeled by 2D periodic microstructures made of an hyperelastic matrix reinforced by rigid fillers with the presence of a cohesive zone at the filler/matrix interface in order to account for possible matrix dewetting at the filler surface. The cohesive zone acts as a spring with damageable stiffness, allowing the matrix/filler adhesion to vary down to null according to the applied loading. The comparison of the behavior of the model composite with experimental data shows the interest of accounting for material damage through a cohesive zone. Moreover, the matrix decohesion from the fillers creates voids that may grow and initiate a fibrillar microstructure favoring strain localization that may be catastrophic. As a consequence an original microstructure failure criterion has been proposed as the appearance of matrix fibrils. A local strain energy criterion was also introduced. The value for such a criterion was chosen in order to coincide with the microstructure failure criterion on one of the simulation.

The microstructure parameters and the constitutive parameters were varied in order to study their impacts on the stress-strain behavior and failure of the model material. When a comparison with actual experimental data was possible, the model seemed to reproduce well the experimental trends. It was confirmed that smaller fillers improves the material properties, and increasing the matrix stiffness benefits to the strain and stress at failure. As for the matrix/filler adhesion, increasing its strength has a mitigate impact, increasing the stress at failure but decreasing the strain at failure, while increasing significantly its toughness (the adhesion energy) improves the stress and strain at failure. The fibrillar microstructure failure criterion seems rel-

evant but is not always reachable. When the damage was well spread across the microstructure, no strain localization was noticed within the matrix. In such a case, the energy criterion was not necessarily relevant since it was reached at larger strain than expected.

Acknowledgments

References

Abaqus/Standard, 2011. Dassault Systèmes Simulia Corporation. Providence, RI, USA.

Brassart, L., Inglis, H. M., Delannay, L., Doghri, I., Geubelle, P. H., 2009. An extended Mori-Tanaka homogeneization scheme for finite strain modeling of debonding in particle-reinforced elastomers. Computational materials science, 45, 611-616.

Camanho, P. P., Davila, C. G., de Moura, M. F., 2003. Numerical simulation of mixed-mode progressive delamination in composite materials. Journal of Composite Materials, 37, 1415-1438.

Dvorak, G.J., Zhang, J., 2001. Transformation field analysis of damage evolution in composite materials. Journal of the Mechanics and Physics of Solids, 49, 2517-2541.

Ghosh, S., Ling, Y., Majumbar, B., Kim, R., 2000. Interfacial debonding analysis in multiple fiber reinforced composites. Mechanics of Materials, 32, 561-591.

Inglis, H. M., Geubelle, P. H., Matouš, K., Tan, H., Huang, Y., 2007. Cohesive modeling of dewetting in particulate composites: micromechanics vs. multiscale finite element analysis. Mechanics of Materials, 39, 580-595.

Matouš, K., Geubelle, P. H., 2006. Finite element formulation for modeling particle debonding in reinforced elastomers subjected to finite deformations. Computational methods in applied mechanics and engineering, 196, 620-633.

Matouš, K., Inglis, H. M., Gu, X., Rypl, D., Jackson, T. L., Geubelle, P. H., 2007. Multiscale modeling of solid propellants: from particles packing to failure. Composites Science and Technology, 67, 1694-1708.

Liu, C. T. , Klynn, L. M., Thompson, J. D., 2004. Monitoring microstructural evolution and crack formation in a solid propellant under incremental strain condition using digital radiography X-ray techniques. Defense Technical Information Center, ADA423473.

Moraleda, J., Segurado, J., Llorca, J., 2009. Effect of interface fracture on the tensile deformation of fiber-reinforced elastomers. International Journal of Solids and Structures, 46, 4287-4297.

Ngo, D., Park, K., Paulino, G.H., Huang, Y., 2010. on the constitutive relation of materials with microstructure using a potential-based cohesive model for interface interaction. Engineering Fracture Mechanics, 77, 1153-1174.

Nie, S., Basaran, C., 2005. A micromechanical model for effective elastic properties of particulate composites with imperfect interfacial bonds. International Journal of Solids and Structures, 42, 4179-4191.

Oberth, A. E., Bruenner, R. S., 1965. Tear phenomena around solid inclusions in castable elastomers. Transaction of the society of rheology, 9:2, 165-185.

Park, K., Paulino, G.H., 2011. Cohesive zone models: A critical review of traction-separation relationships across fracture surfaces. Applied Mechanics Reviews, 64, 060802.

Rivlin, R. S., Thomas, A. G.,1953. Rupture of rubber. I. Characteristic energy for tearing. Journal of polymer science, 10, 291-318.

Safranski, D., Gall, K., 2008. Effect of chemical structure and crosslinking density on the thermo-mechanical properties and toughness of (meth)acrylate shape memory polymer networks. Polymer, 49, 4446-4555.

Tao, Z. J.,Ping, S. D., Mei, Z., Cheng, Z. P., 2013. Microstructure deformation and fracture mechanism of highly filled polymer composites under large tensile deformation, 12th International Symposium on Multiscale, Multifunctional and Functionaly Graded Materials, IOP Science.

Tan, H., Huang, Y., Liu, C., Ravichandran, G., Inglis, H. M., Geubelle, P. H., 2007. The uniaxial tension of particulate composite materials with nonlinear interface debonding. International Journal of Solids and Structures, 44, 1809-1822.

Tan, H., Liu, C., Huang, Y., Geubelle, P. H., 2005. The cohesive law for particle/matrix interfaces in high explosives. Journal of the Mechanics and Physics of Solids, 53, 1892-1917.

Torquato, S., 2002. . Random heterogeneous materials, Springer.

Torquato, S., Lado, F., 1985. Characterisation of the microstructure of distributions of rigid rods and discs in a matrix. Journal of Physics A: Mathematical and General, 18, 141-148.

Tvergaard, V., Hutchinson, J. W., 1993. The influence of plasticity on mixed mode interface toughness. Journal of the Mechanics and Physics of Solids, 41, 1119-1135.

Vratsanos, L. A., Farris, R. J., 1993a. A predictive model for the mechanical behavior of particulate composites. Part I: Model derivation, Polymer Engineering and Science, 33, 1458-1465.

Vratsanos, L. A., Farris, R. J., 1993b. A predictive model for the mechanical behavior of particulate composites. Part II: Comparison of model predictions to literature data, Polymer Engineering and Science, 33, 1466-1474.

Yilmazer, U., Farris, R.J., 1983. Finite element formulation for modeling particle debonding in reinforced elastomers subjected to finite deformations, Journal of Applied Polymer Science, 28, 3369-3280.

Zhong, X. A., Knauss, W. G., 1997. Analysis of interfacial failure in particle-filled elastomers, Journal of Engineerig Materials and Technology, 119, 198-204.

Zhong, X. A, Knauss, W. G., 2000. Effects of particle interaction and size variation on damage evolution in filled elastomers, Mechanics of composite materials and structures, 7, 35-53.